25th ABCM International Congress of Mechanical Engineering
October 20-25, 2019, Uberlândia, MG, Brazil

# COB-2019-0147
# DETERMINATION OF PROCESSING PARAMETERS WINDOW FOR LASER CLADDING OF IRON AND TIN ALLOY

**Gustavo Henrique Truppel**
**Milton Pereira**
**Paulo Antônio Pereira Wendhausen**
Universidade Federal de Santa Catarina, Departamento de Engenharia Mecânica – Florianópolis/SC – Brazil
gustavo.truppel@posgrad.ufsc.br
milton.pereira@ufsc.br
paulo.wendhausen@ufsc.br

***Abstract.*** *Hydrodynamic bearings of rotating machines can develop wear behaviors that cause failures and reduction in productivity. For this, tin-based metal alloys are used as bearings coatings since they can improve tribological properties. This work studies the laser power and traverse speed influence on geometric dilution results of Fe and Sn-based deposits processed by laser cladding. Experimental methodology presented single-tracks bead-on-plate depositions with different combinations of laser power and traverse speed, which varied four levels each. The experiments results were accessed through tracks' cross sections analyses made by Scanning Electron Microscope (SEM) and Energy Dispersive X-ray Spectroscopy (EDS). It was concluded that a geometric dilution behavior was only achieved by the highest power level, independently of the traverse speed. With this, the lowest geometric dilution achieved (14.41%) was presented by a combination of 1400 W with 5 x $10^{-3}$ m/s. EDS element mapping presented a homogenous microstructure composed by Fe and Sn-rich phases. Therefore, it can be concluded that future optimization work aiming an even lower dilution level must explore a process parameter window around 1400 W and 5 x $10^{-3}$ m/s.*

***Keywords:*** *laser cladding; Tin-alloy; Dilution; Microstructure; Process window.*

## 1. INTRODUCTION

Hydrodynamic bearings of rotating machines used in industrial processes develop, under specific conditions, wear behaviors which cause failures during operation (Mendes; Machado; Cavalca, 2017). In order to avoid wear and economic losses, alternatives of surface modification can be proposed. Covering a steel with a dissimilar substance can reach conditions that foment the hypothesis of up scaling the process technique to industrial application (Ya *et al.*, 2018).

Tin-based metal alloys are used as bearings coatings since they can improve tribological properties. Alcover Junior and Pukasiewicz (2019) and Nascimento *et al.* (2017) analyzed centrifugal, casting, HVOF (High Velocity Oxygen Fuel), arc and flame spraying processes to deposit tin-based alloys and, then, concluded that the challenges to ensure quality are related to intermetallic structures and porosity formations, which are functions of the cooling and solidification rates. Therefore, the cited fabrication methods can show negative characteristics, such the need of pre-treatments, porosity high level and no metallurgical bonding with the substrate.

Laser cladding technique based on a coaxial powder feeder has a laser beam that plays the role of energy source, aiming a molten pool formation which arises when the beam interacts with the substrate. Thus, the additional material is conveyed to the melt pool region and, upon relative movement between the laser-head and the working-table, a deposition track is produced. When these tracks are deposited laterally to one another, a layer is created. The addition of these layers over other layers brings the formation of the desired component. This manufacturing methodology is a considerable deposition alternative, as it shows high cooling rates of the melt pool, assigned with dense components and suitable deposition rates (Thompson *et al.*, 2015).

The use of a material feed system in conjunction with a drive system and a laser beam provides many process parameters combinations that guides the interaction conditions between the energy source and processing materials. Shah *et al.* (2014) studied the influence of laser power on the macrostructure and dimensions of 316 L and Inconel 718 stainless steel powder layer depositions. Kummailil *et al.* (2005) experienced variations in laser power and traverse speed to study their relationships with results in terms of Ti-6Al-4V layer depositions height. Recently, Jinoop, Paul and Bindra (2019) analyzed the influence of power and traverse speed parameters on the deposition rate of Hastelloy-X

layers. Therefore, it is possible to conclude that the research between the relation of parameters, process and materials properties is necessary for results optimization.

Laser cladding process manufactures metallic components by overlaying layers from a defined substrate. Ramakrishnan and Dinda (2019) cite in their work that, in order to guarantee metallurgical bonding, first layers are processed with a power of 1000 W, and each layer overlaid is reduced in 50 W until the power level of interest. Shah *et al.* (2014) also showed special care with the initial layers as they controlled material composition over layers depositions until a desired composition was established. Olakanmi *et al.* (2019) investigated laser power values along with traverse speed and correlated relatively low dilution results (about 7%) with metallurgical and mechanical properties. Thus, the deposition parameters related to first layers on the substrate present relevant aspects in the fabricated material properties, since these initial layers must meet certain requirements and assume, in a certain way, a transition role between the substrate and the component of interest.

Since studies with an approach between laser cladding, tin-alloys, geometric dilutions and microstructure analysis were not found in the literature, the present work studies and analyzes the relation between these factors. A specific objective is to determine a process parameter map that divides the geometric dilution evolution according to the conditions. Then, a parameter window that correlates a suitable geometric dilution level with proper deposition characteristics is pointed out, so this can serve as basic data for future optimization steps.

## 2. METHODOLOGY

### 2.1 Materials

The deposition substrate was a laminated SAE 1020 sheet (length, width and thickness of 200, 50 and 10 x $10^{-3}$ m, respectively). Prior to the tests, plates were sandblasted and cleaned to remove oxides and surface impurities. The deposited material was a mixture of iron powder AHC 100.29 from Höganas® (particle size between 20 and 200 µm and irregular morphology) and a silver and tin alloy of Heraeus® (particle size between 15 and 35 µm and rounded morphology). Before mixing, Fe powder was sieved by a 106 µm mesh. Figure 1 shows the powder mixture morphology and particle size distribution. For the tin alloy powder, 3.5% by weight is silver and the remainder is tin. The powder mixture (Fe + Sn-Ag) had a nominal composition of 80% iron and 20% tin-silver alloy (percentage by mass). Powder mixture showed a granulometry average of 68.40 x $10^{-6}$ m, with a flowability of 24.84 ± 0.71 s and apparent density of 3.43 ± 0.02 g/cm³.

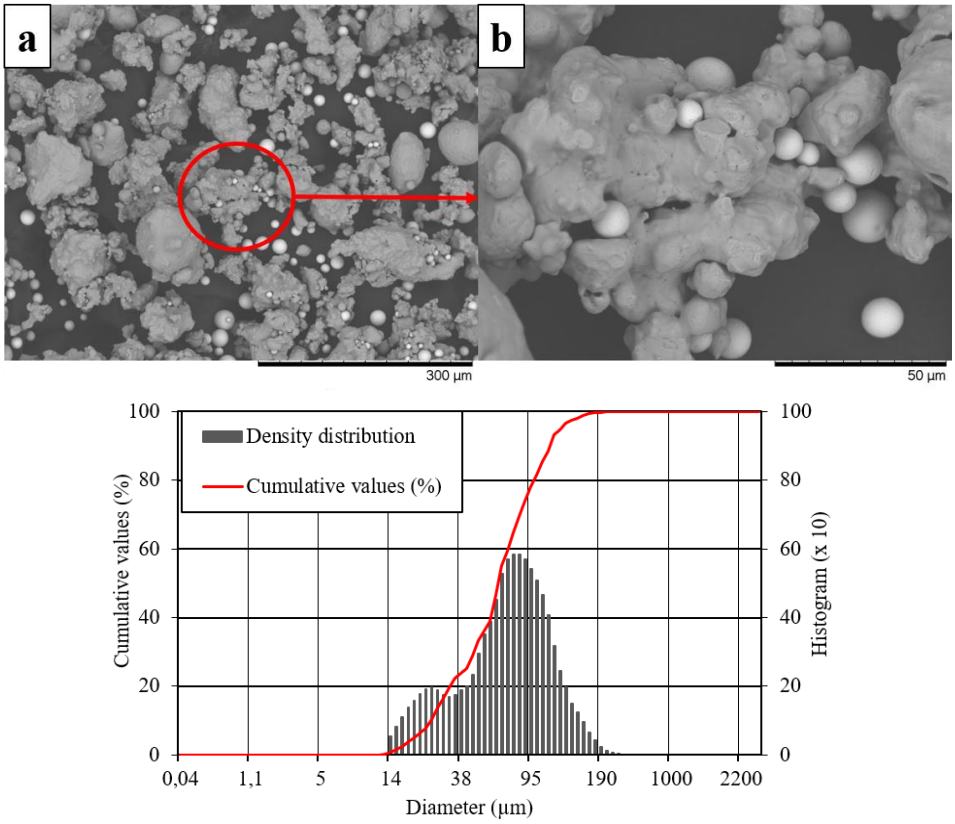


Figure 1 – Powder mixture morphology (a and b) and cumulative values (%) and density distribution (c).

## 2.2 Equipment

Tests were performed with a high power (up to 10 kW) YLS-10000 laser source from IPG Photonics®. The source contains a fiber laser (Yb, Ytterbium) with wavelength in the range of 1070 to 1080 x $10^{-9}$ m. A powder feeder unit from GTV® is used. The feeder system consists of a powder reservoir and a conveyor system (disc with grooves, which rotates at a certain speed per minute, controlling the feed rate). Powder is then fed coaxially to the laser beam by a cladding nozzle COAX-50-S from Fraunhofer ILT, which is coupled to a YW52 Precitec® head. A Siemens® CNC SINUMERIK 840D SL drive system is adopted for work-table motion. The equipment is showed by Fig. 2.


Figure 2 – Equipments used in the experiments: a) laser source, b) powder feeder system, c) cladding head and d) CNC command unit.

## 2.3 Experimental procedure

Experiments methodology was made up of two factors: laser power (*P*) and traverse speed (*V*). However, the objective of the study is not to quantify or compare the means or effects that these factors exert in terms of dilution, but to analyze their trends and identify parameters combinations that generate dilution conditions. Therefore, both *P* and *V* varied in 4 levels, generating 16 different combinations. Similar to other authors (Dos Santos Paes *et al.*, 2018), it is assumed that laser has good repeatability and, therefore, a consistent trend significance can be observed even when the variance of the results is ignored since it is considered low. Then, repetitions were not considered. Table 1 shows the adopted parameters. Each sample number represents a track linearly deposited on the steel sheet. For all depositions, the material feed rate (1.67 x $10^{-4}$ kg/s, equivalent to 10 g/min), carrier gas flow (8.33 x $10^{-5}$ $m^3$/s, equivalent to 5 l/min), shielding gas flow (2.5 x $10^{-4}$ $m^3$/s, equivalent to 15 l/min) and focal length of the laser beam to the substrate (35 x $10^{-3}$ m) are kept constant. Low values of dilution are considered positive features.

## 2.4 Results assesment

In order to evaluate the microstructures and geometric dilutions characteristics of deposited tracks, all samples were sectioned transversally in their central regions and passed through a metallographic process. They were cold embedded (polymer resin), sanded (80 to 1200 mesh sands) and polished (1 x $10^{-6}$ m alumina). Tracks' macrographs, micrographs

and element mapping were performed on a Hitachi® TM3030 Scanning Electron Microscope (SEM) with a Hitachi® SwiftED 3000 Energy Dispersive X-ray Spectroscopy (EDS) coupled. Then, geometric dilution values were measured using ImageJ software according to Eq. (1), as its method is illustrated by Fig. 3.

$$\text{Geometric Dilution} = \frac{\text{Penetration area}}{\text{Penetratiom area} + \text{Reinforcement area}} \quad (1)$$

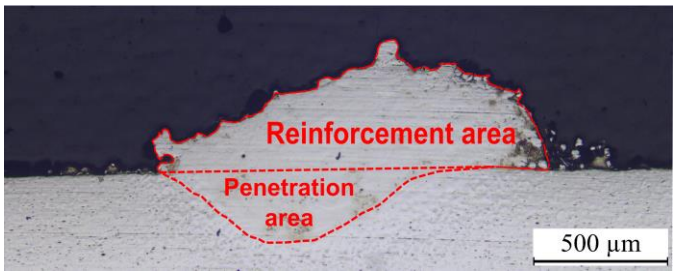


Figure 3 – Dilution measurement example from a deposited track cross section.

## 3. RESULTS

Figure 4 shows depositions' top views. From this figure, it can be seen that tracks tend to become wider as *P* increases, independently of *V*. In an opposite way, greater values of *V* induce to tracks' width reduction, independently of *P*. However, Fig. 4 suggest that the width-increasing effect due to an enhanced *P* is greater than the width-decreasing effect due to an enhanced *V*. Figure 4 also points out that higher levels of *P* induced to higher deposition rates, while *V* reduced it. These informations are confirmed by Fig. 5.

Table 1 shows the parameters adopted and the dilution results. It is observed that dilution profiles were achieved only in the highest level of *P* (1400 W), independently of *V* values. This characteristic can be justified by the fact that, considering a constant *V*, higher levels of laser power enhances the thermal energy imposed in the process. In addition, considering a constant *P* of 1400 W, Tab. 1 also shows that the higher the traverse speed, the higher the dilution value.

Table 1 - Process parameters analyzed and results of dilution.

| Sample Number | *P* (W) | *V* x $10^{-3}$ (m/s) | Dilution (%) |
|---|---|---|---|
| 1 | 350 | 5.00 | 0.00 |
| 2 | 700 | 5.00 | 0.00 |
| 3 | 1050 | 5.00 | 0.00 |
| 4 | 1400 | 5.00 | 14.41 |
| 5 | 350 | 13.33 | 0.00 |
| 6 | 700 | 13.33 | 0.00 |
| 7 | 1050 | 13.33 | 0.00 |
| 8 | 1400 | 13.33 | 20.91 |
| 9 | 350 | 21.67 | 0.00 |
| 10 | 700 | 21.67 | 0.00 |
| 11 | 1050 | 21.67 | 0.00 |
| 12 | 1400 | 21.67 | 21.53 |
| 13 | 350 | 30.00 | 0.00 |
| 14 | 700 | 30.00 | 0.00 |
| 15 | 1050 | 30.00 | 0.00 |
| 16 | 1400 | 30.00 | 24.31 |

Figure 5 justifies the reason of achieving higher values of dilution when *V* is increased with a constant *P*. It shows values of reinforcement and penetration areas as functions of *P* and *V*. From Fig. 5a, it is possible to observe that the reinforcement area is reduced as *V* is enhanced and *P* remains the same. Figure 5b also shows a reduction behavior (but only for the highest *P*, 1400 W). Comparing Fig. 5a and 5b, it is possible to see that the reinforcement area is reduced

more significantly than the penetration area. To a certain degree, a correlation between Tab. 1 and Fig. 5 illustrates that the dilution has also a dependency on deposition rate, which would affect the reinforcement area and could also be controlled by the powder feed rate parameter. Figure 5a also shows that, when *P* was set with 350 W, the reinforcement area was not strongly affected by the *V* parameter as it was when processed with higher values of *P*. No penetration was achieved with *P* values below 1400 W and, for this, Fig. 5b only shows results of samples with 1400 W.

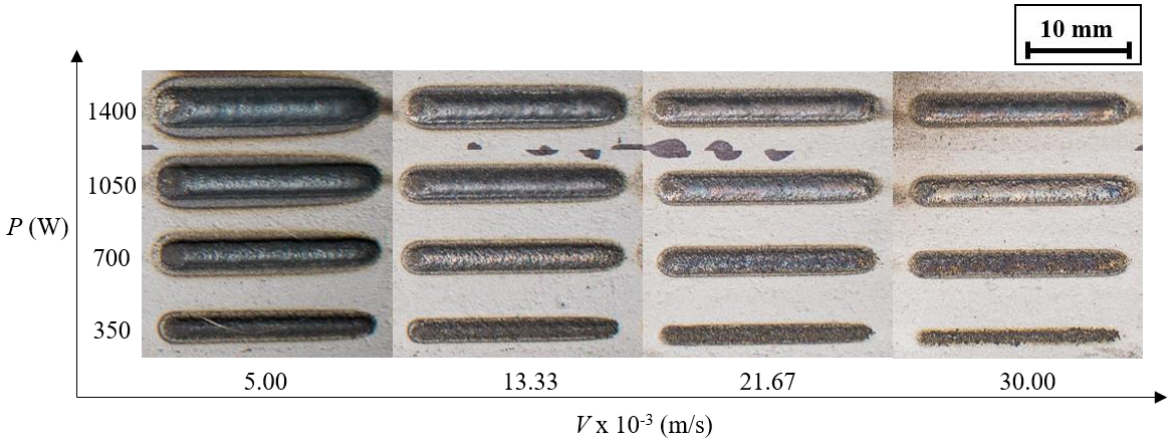


Figure 4 – Top views from depositions numbered in Tab. 1.

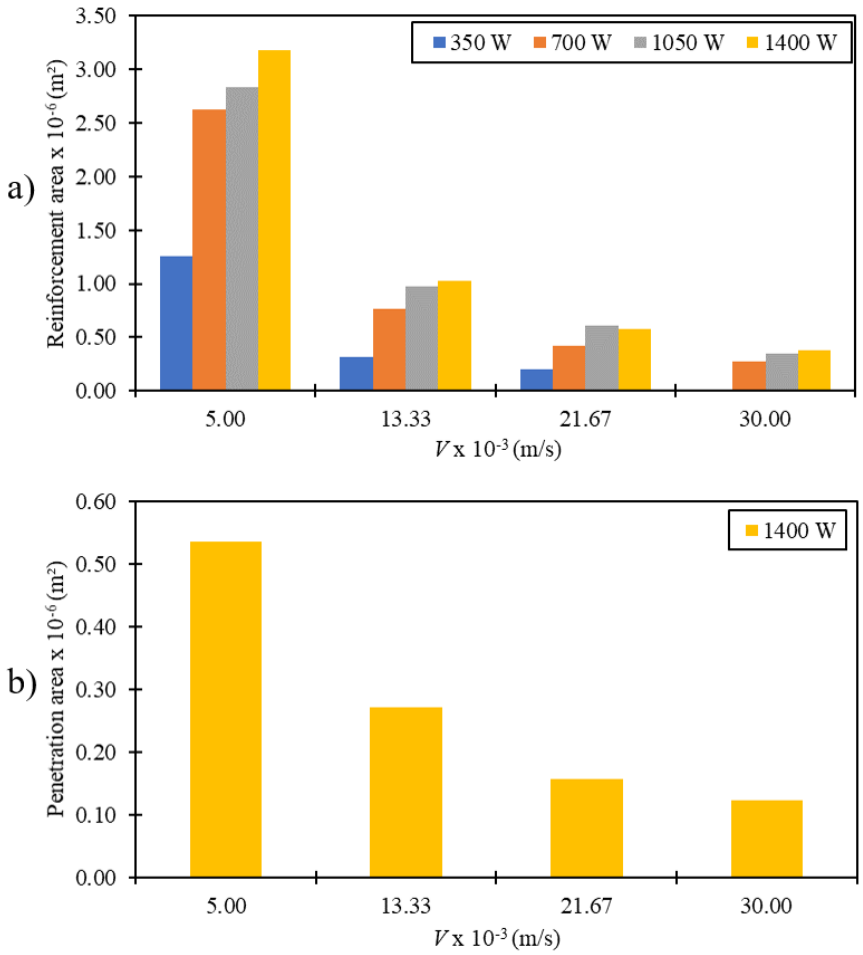


Figure 5 - a) Reinforcement area (m²) and b) Penetration area (m²) as functions of *P* (W) and *V* (m/s).

Sample number 4 presented the biggest reinforcement area (3.18 x $10^{-6}$ m²) with a relatively small penetration area (0.54 x $10^{-6}$ m²) and, then, resulted in the track with the lowest geometric dilution (14.41%). Figure 6 shows final

microstructure from sample number 4 after processing. Such images were acquired by SEM using the Backscattered Electrons (BSE) contrast.

It is considered that BSE images from EDS analyses show Sn-rich areas with lighter colors than Fe (Sn atoms are heavier than Fe ones). Then, it is possible to observe a microstructure with a fine grain morphology, with an iron-rich phase (gray color) distributed with a tin-rich phase (white color). Little black points are also observed and can be related to metallurgical defects (pores), oxidation pits or even a material portion removed during polishing. However, their reasons and discussions are disregarded in this work, since the objective is not to set optimum parameters.

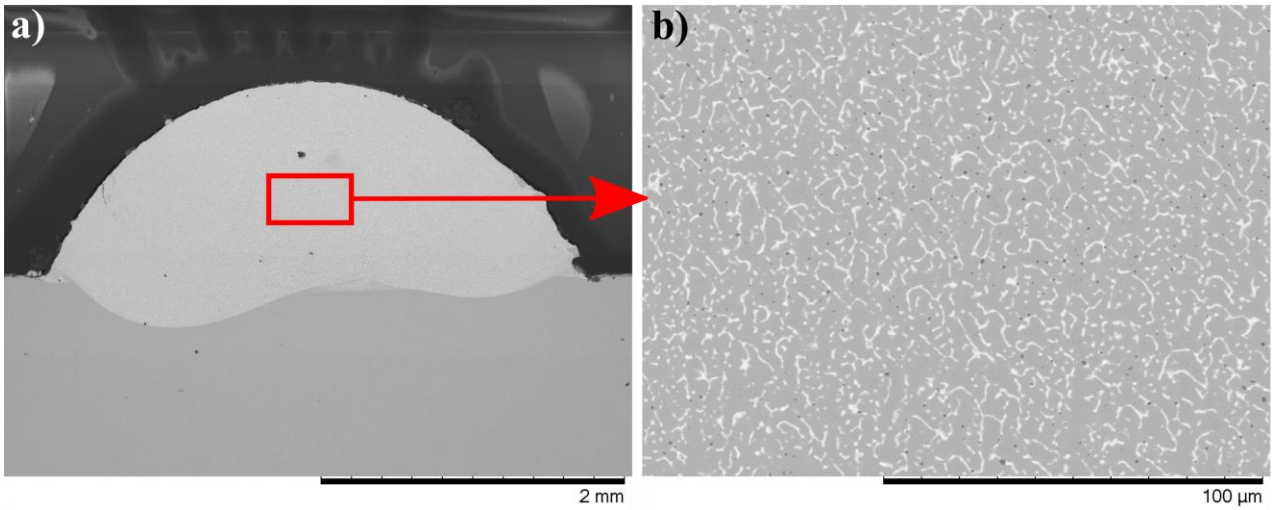


Figure 6 – a) Sample number 4 cross section macrograph made by SEM and b) magnification of image “a”.

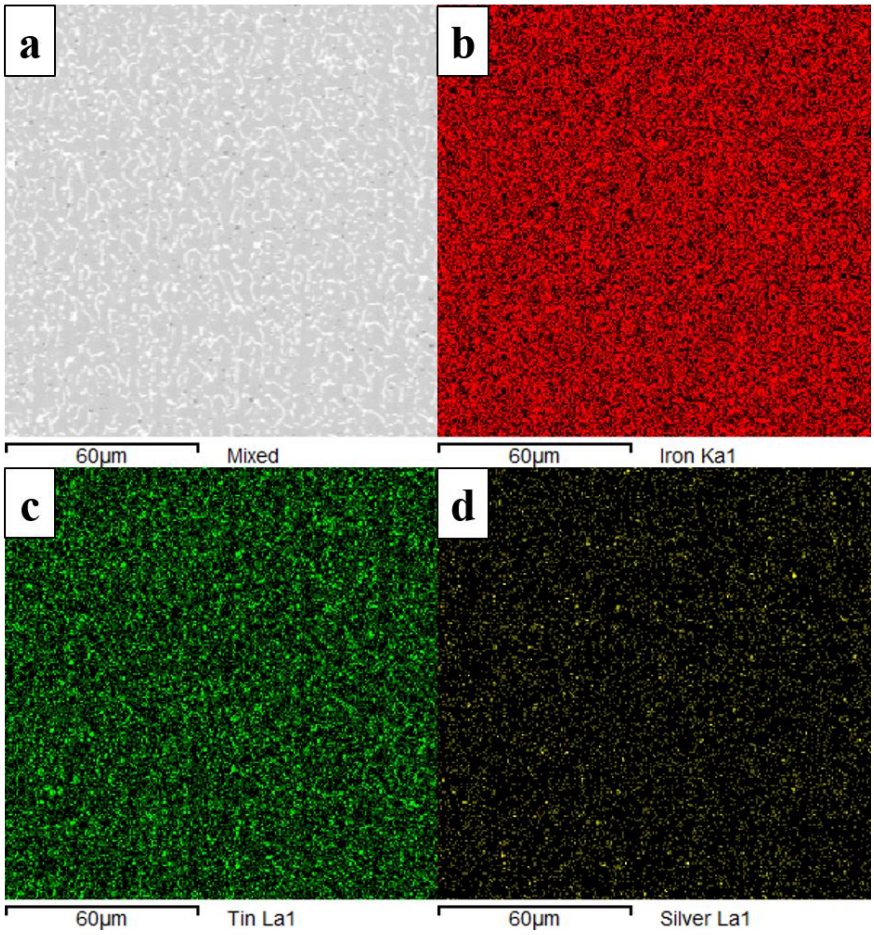


Figure 7 – EDS element analysis of sample number 4 showing the a) standard image and maps of b) iron, c) tin and d) silver. Images had a magnification of 1000x.

An element map made through EDS (Fig. 7) revealed that the microstructure observed on the track cross section from sample number 4 has a homogenous element distribution, since no significant macro segregation of iron, tin or silver is observed. This resultant microstructure suggests that both iron and tin-based powders melted after heating and, later, solidified. If there were iron particles not being melted during deposition process, microstructure aspects would show EDS element maps with sharp, well-defined Fe and Sn rich areas. Future X-Ray Diffraction (XDR) analysis can confirm microstructure phases, but it is expected that Sn solid solution in Fe-α and Fe-Sn intermetallics were formed.

## 4. CONCLUSIONS

The geometric dilution of deposited tracks is a function of laser power and traverse speed. Experiments showed that the higher the *P* parameter, the greater is the tendency of achieving dilution. Analogously, for higher ranges of *V* and a constant *P* of 1400 W, tendency is also for an enhanced dilution. Parameters *V* and *P* influence the resulting reinforcement areas, generating a strong reduction trend. Both *V* and *P* also influence results of penetration areas, but in a subtle way. Another interesting behavior is that *V* tends to influence more when the material is processed with higher ranges of *P*.

Thus, considering the process conditions, it was possible to conclude that a dilution behavior was only achieved by the highest power level, independently of the traverse speed. With this, the lowest dilution value achieved (14.41%) was a result from the combination of 1400 W of 5 x $10^{-3}$ m/s. EDS element analysis presented a homogenous microstructure composed by Fe and Sn-rich phases. Then, it is concluded that future optimization research aiming a lower dilution level must have a process parameter window around 1400 W and 5 x $10^{-3}$ m/s.

## 5. ACKNOWLEDGEMENTS

Authors thank the National Council for Scientific and Technological Development (CNPq) and Mechanical Engineering Post-Graduation Program (POSMEC – UFSC) for the support. In addition, special acknowledgements to the groups from UFSC for the material and infrastructure supply: LabMat (materials laboratory), MAGMA (magnetic materials group from LabMat) and LMP (precision engineering laboratory).

## 6. REFERENCES

Alcover Junior, P. R. C.; Pukasiewicz, A. G. M. Evaluation of microstructure, mechanical and tribological properties of a Babbitt alloy deposited by arc and flame spray processes. *Tribology International*, v. 131, p. 148–157, Mar. 2019.

Dos Santos Paes, L. E. *et al.* Comparison of methods to correlate input parameters with depth of penetration in LASER welding. *The International Journal of Advanced Manufacturing Technology*, 14 Nov. 2018.

Jinoop, A. N.; Paul, C. P.; Bindra, K. S. Laser assisted direct energy deposition of Hastelloy-X. *Optics & Laser Technology*, v. 109, p. 14–19, Jan. 2019.

Kummailil, J. *et al.* Effect of Select LENS™ Processing Parameters on the Deposition of Ti-6Al-4V. *Journal of Manufacturing Processes*, v. 7, n. 1, p. 42–50, Jan. 2005.

Mendes, R. U.; Machado, T. H.; Cavalca, K. L. Experimental wear parameters identification in hydrodynamic bearings via model based methodology. *Wear*, v. 372–373, p. 116–129, Feb. 2017.

Nascimento, A. R. C. *et al.* Production of Babbitt Coatings by High Velocity Oxygen Fuel (HVOF) Spraying. *Journal of Thermal Spray Technology*, v. 26, n. 7, p. 1732–1740, 22 Oct. 2017.

Olakanmi, E. O. *et al.* Multi-variable optimisation of the quality characteristics of fiber-laser cladded Inconel-625 composite coatings. *Surface and Coatings Technology*, v. 357, p. 289–303, Jan. 2019.

Ramakrishnan, A.; Dinda, G. P. Direct laser metal deposition of Inconel 738. *Materials Science and Engineering: A*, v. 740–741, p. 1–13, Jan. 2019.

Shah, K. *et al.* Parametric study of development of Inconel-steel functionally graded materials by laser direct metal deposition. *Materials & Design (1980-2015)*, v. 54, p. 531–538, Feb. 2014.

Thompson, S. M. *et al.* An overview of Direct Laser Deposition for additive manufacturing; Part I: Transport phenomena, modeling and diagnostics. *Additive Manufacturing*, v. 8, p. 36–62, 2015.

Ya, W. *et al.* Cladding of Tribaloy T400 on steel substrates using a high power Nd:YAG laser. *Surface and Coatings Technology*, v. 350, p. 323–333, Sep. 2018.

## 7. RESPONSIBILITY NOTICE

The authors are the only responsible for the printed material included in this paper.